

Thermal Fatigue of High-Heat-Load Synchrotron Components

V. Ravindranath (1), S.Sharma (1), B.Rusthoven (2), J.T. Collins (2)

(1)National Synchrotron Light Source II, Brookhaven National Laboratory, Upton, NY 11973-5000, USA

(2)Advanced Photon Source, Argonne National Laboratory, Argonne, IL 60439, USA

Abstract

Photon absorbers, masks, and shutters made of Glidcop Al-15 are exposed to intense thermal stress from high-intensity x-ray beams at third-generation light sources. This paper presents our findings at the APS where we assessed the thermal-fatigue lifespan of Glidcop specimens exposed to 10,000 thermal cycles of an undulator x-ray of three different power densities of 105, 115, 125 W/mm². The peak temperatures in the centre of the footprint at these power densities were 500, 550, and 600 Deg C, respectively. Optical microscopy revealed that the sample exposed to 600 Deg C developed sub-surface thermal fatigue cracks of 1.6 mm depth that was deemed to be unacceptable due to the proximity of the cracks to the cooling channels. The samples subjected to 500 and 550 Deg C peak temperature rises had much smaller sub-surface cracks ranging from 0.025 to 0.3 mm. In this work a non-linear finite element methodology was also used to model the thermal fatigue behavior of the high-heat-load components. The numerical model was calibrated based on the experimental results and a fatigue life of 19,000 cycles was predicted for samples exposed to a power density of 94 W/mm², resulting in a peak temperature of 450 Deg C. Follow-up thermal fatigue experiments revealed that one sample exposed to this power density survived 20,000 thermal cycles with minimal cracking (maximum crack depth was 0.01 mm), while another sample with several surface defects but half the number of thermal cycles (10,000 cycles), developed 0.33 mm deep cracks.

1. Introduction-Background

Third generation light sources, such as the Advanced Photon Source (APS), generate extremely powerful x-rays. To control the exposure of downstream components to these intense rays, these facilities use many critical components, such as photon absorbers, masks, and shutters, which are water cooled, and usually made from Glidcop Al-15, a dispersion-strengthened copper containing 0.15% submicroscopic alumina particles. This material has a much higher yield-strength, ultimate tensile-strength, fatigue-strength, and rupture-strength at elevated temperatures than does Oxygen-free High Conductivity (OFHC) copper. Since the thermal conductivity of both is similar, Glidcop is an excellent material for high-heat-load applications [1].

Fig.1 depicts the average temperature fluctuations experienced by the critical components at these light sources. Two major mechanisms can severely affect their service life; thermal-fatigue, and the dwell-time effect. The former is the gradual deterioration and eventual cracking of a material caused by alternate heating and cooling during which free thermal-expansion is partially or completely constrained.

The second mechanism, dwell-time effect, refers to a material's degradation that occurs under a prolonged constant load, especially at elevated temperature. As reported, dwell-time damage in material usually is caused by creep phenomenon (internal sliding of grains along the grain boundaries) [2], environmental reactions, such as oxidation [3], and stress relaxation [4].

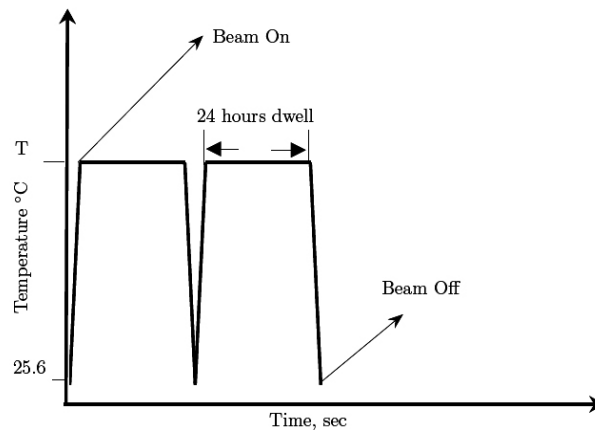


Figure 1. Schematic figure depicting the average temperature fluctuations experienced by the critical components at the light sources.

Under pure thermal loading (lacking mechanical loading) creep-induced damage in the light-source components does not occur at ambient temperature; then, the dwell-time effect can be ignored unless they are exposed to an x-ray beam. Even then, the localized stresses that develop in them are compressive ones, and will only aid in closing pre-existing cracks. Hence, we assume that creep phenomenon will not significantly change the components' life spans. Similarly, we also can rule out any effect of oxidation on their service life because the components are held under vacuum. However, stress relaxation, an indirect effect of creep in material, can be detrimental to them. Stress relaxation refers to the phenomenon in which the stresses in a material experience load relax due to creep at elevated temperatures; when this load is removed or its direction reversed, residual stresses build up as an indirect after-effect. Should they be tensile ones then pre-existing cracks will open up, enhancing the growth of the cracks, and finally leading to the component's failure.

In this phase of study, our goal was to establish a safe operating condition in terms of the power density under which the Glidcop components used at the light sources can survive 10,000 cycles of exposure to the beam. In the typical Glidcop component employed, the thermal stresses generated in the component are purely from the thermal constraint due to localized heating, in which a portion of the component's surface exposed to the beam is at a higher temperature than the rest of its surface. To simulate this condition, we devised a test plan in which Glidcop samples were cyclically exposed to an x-ray beam at a 90° beam incidence angle. Each half of the thermal-load cycle lasted 30 seconds (heating during beam exposure and cooling during beam-off conditions) based on thermal-FEA analyses showing that this material reaches a steady-state temperature condition in that time. In addition to the experimental work, we developed a numerical model to estimate fatigue life, which we discuss in detail in this paper. We did not address the effects of stress relaxation/dwell time; it is a topic for future work.

2. Thermal-fatigue Experiments

2.1. Experimental Setup

In considering temperature effects on the fatigue life-span of Glidcop Al-15, we carried out the following tests at the APS: (a) 10,000 cycles of exposure on one sample at 600 °C; (b) 10,000 cycles of exposure on two samples at 550 °C, (c) 10,000 cycles of exposure on one sample at 500 °C, and (d) 10,000 cycles of exposure on two samples at 450 °C

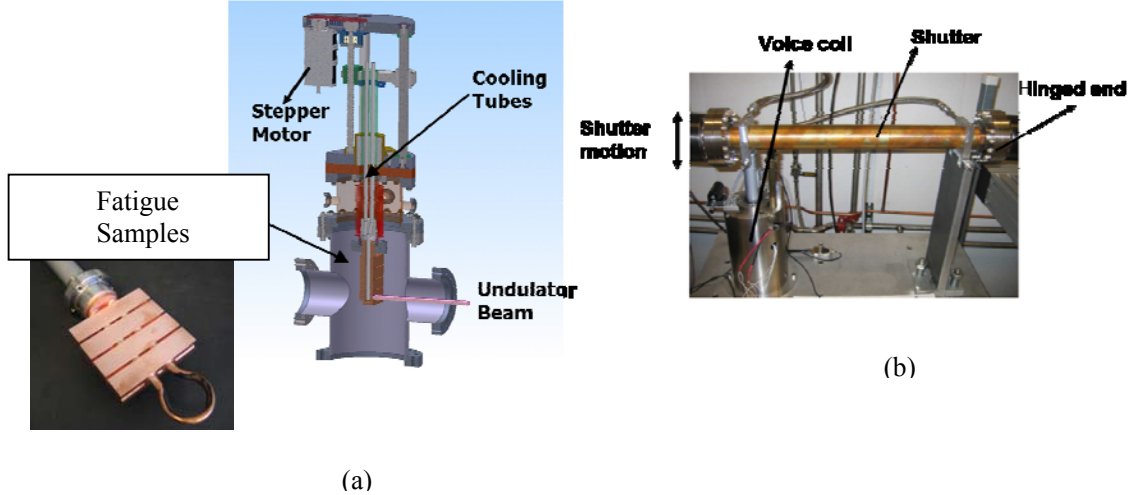


Figure 2. Thermal-fatigue experimental set-up at the APS. (a) Cyclic exposure to an x-ray beam was achieved by moving all four samples up and down via the stepper motor. The exposure time per sample was 30 seconds, (b) Actuating shutter used for thermal cycling at the APS

The test set-up (Fig. 2) consisted of an upstream actuating shutter that imposed the cyclic thermal-loading conditions. As Fig.2 (b) shows, a hinge at one end of the shutter allowed it to swivel while its other end was connected to a voice-coil, i.e., an electro-magnetic linear actuator. To actuate the shutter, we used Compumotor's programmable closed-loop GV-6K servo controller, sequencing it so that the shutter remained horizontal for 30 seconds during which time the downstream specimen was exposed to the x-ray beam, as depicted in Fig.3. Then, the shutter closed to intercept the x-ray beam for 30 seconds, thereby allowing the specimen to cool to the temperature of the inlet water.

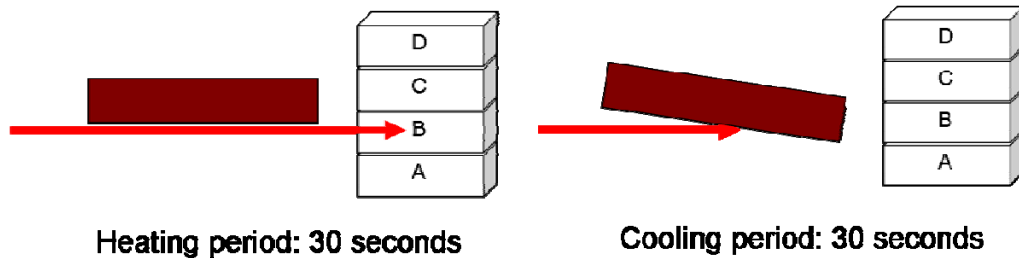


Figure 3. Schematic representation of the thermal-fatigue experiment at the APS. Each sample was cyclically exposed to an x-ray beam by manipulating the upstream shutter that was programmed to allow beam exposure for 30 seconds, and then was closed to intercept the beam for 30 seconds.

A separate OFHC copper tube with an internal diameter of 9.625 mm brazed to the specimens supplied them with cooling water. Thus each sample was exposed to the beam for 10,000 cycles and then the set of samples was moved vertically via the stepper motor, thus allowing the initial positioning of the specimen for each test. The thermal-fatigue experiments at the APS were carried out in Sector 26-ID beam-line that receives an x-ray beam from two type-A in-line undulators. Table1 lists the undulator's relevant parameters [5].

Table 1 Parameters of Undulator A

Parameter	Values
Beam current	100 mA
Relativistic gamma	13700
Number of periods	144
Period length	3.3 cm
Undulator length	2.4 m
Minimum Undulator gap	11 mm
Horizontal Beam size (sigx)	0.275 mm
Vertical Beam size (sigy)	0.009 mm
Horizontal Beam divergence (sigx')	0.0113 rad
Vertical Beam divergence (sigy')	0.003 rad

To obtain the undulator-gap values corresponding to the test temperatures, we assessed the beam-power experienced by a sample sited 35 m from the undulator's source. A 2 mm x 2 mm exit mask at 25 m from the source restricts the beam's size on the samples to 2.8 mm x 2.8 mm. We approximated the beam's Gaussian profile by a uniform heat flux; the beam-power values corresponding to the test temperatures were obtained from a steady-state thermal-finite element analysis. Column 2, Table 2 presents these computed power values.

Table 2 Undulator gaps and beam power corresponding to the estimated test temperatures

Expected Temperature (°C)	Peak Power Density (W/mm ²)	Absorbed Power (W)	Adjusted Power (W)	Undulator Gap (mm)
600	125	986	1183	14.3
550	115	904	1085	15.1
500	105	823	987	15.6
450	84	660	828	16.5

Based on observations from similar thermal fatigue experiments carried out at ESRF [6], we increased the computed beam-power values by 20% (listed in column 3, Table 2) to account for the loss in beam power due to scattering. Column 4 gives information on the undulator-gap corresponding to these higher values (Personal communication, R.J. Dejus). We verified the estimated undulator-gap values for the required test temperatures were verified by adjusting the undulator gap and then measuring the rise in the temperature of the cooling water flowing through the specimen. From the measured water temperature, the absorbed thermal power was computed using the following expression:

$$Q = \dot{m} C_p \Delta T \quad (1)$$

where Q is the thermal energy or power in Kilo Watts, \dot{m} is the mass flow rate of the cooling water = 0.206 Kg/s, C_p is the specific heat of water = 4.176 KJ/kg-K, and ΔT is the water's temperature differential in °C. To accurately measure the temperature rise in the cooling water, we installed a T-

type thermo-couple manufactured by Omega Engineering (model N.O. TMQSS-125U-6) in the line supplying cooling water to the specimens, placing it less than 300 mm away from the vacuum test chamber enclosing the specimens. The power computed via Eq.2 and shown in column 3 of Table 3 matches the estimated power shown in column 4; there is 3-4% difference between them. Since beam-power and temperature are linearly related, we expect the same percentage difference in the temperature values.

Table 3 Comparison between the power computed by measuring the temperature differential of cooling water and the estimated power

Undulator Gap (mm)	Water Temperature Rise (°C)	Computed Power (W)	Estimated Power (W)	Difference (%)
14.3	1.1	947.42	986	4
15.6	1.0	861.30	823	4.4
17.5	0.8	689.03	660	4.3

2.2. Results of Thermal-fatigue Experiments

For each sample, we intermittently stopped thermal cycling after every 1000 cycles, and visually inspected it for surface cracks via the view port in the test chamber, employing a survey alignment scope with a magnification of 40. Distinct crack-type features were evident on the surfaces (Fig.4) that were more prominent for the sample exposed to a peak temperature of 600 °C.

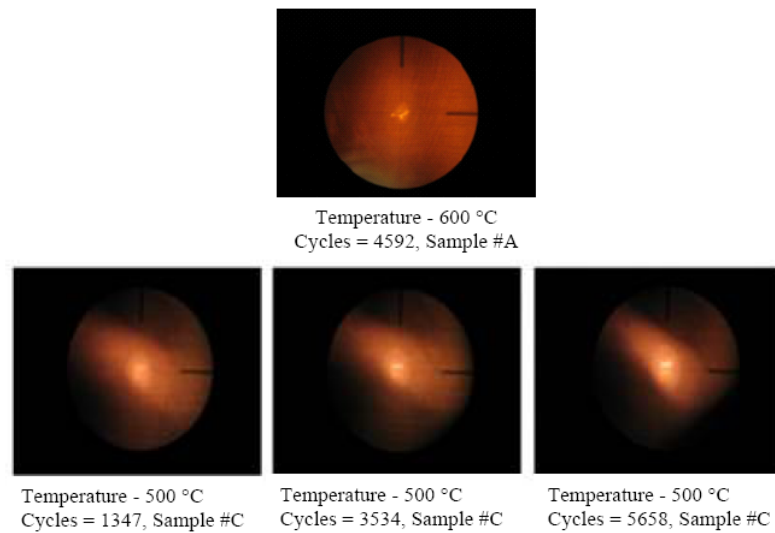


Figure 4. Appearance of APS samples after various thermal cycles.

After 10,000 cycles, the four samples were analyzed by optical microscopy at the ATRONA Metallurgical Laboratory using test coupons containing the beam-exposed area from each of them. To determine the depth of thermal-fatigue cracks, we examined the plane perpendicular to the exposed surface. Fig.5 a-f shows, respectively, both the surface cracks and their depths in the perpendicular plane for peak test temperatures of 600-, 550- and 500 -°C.

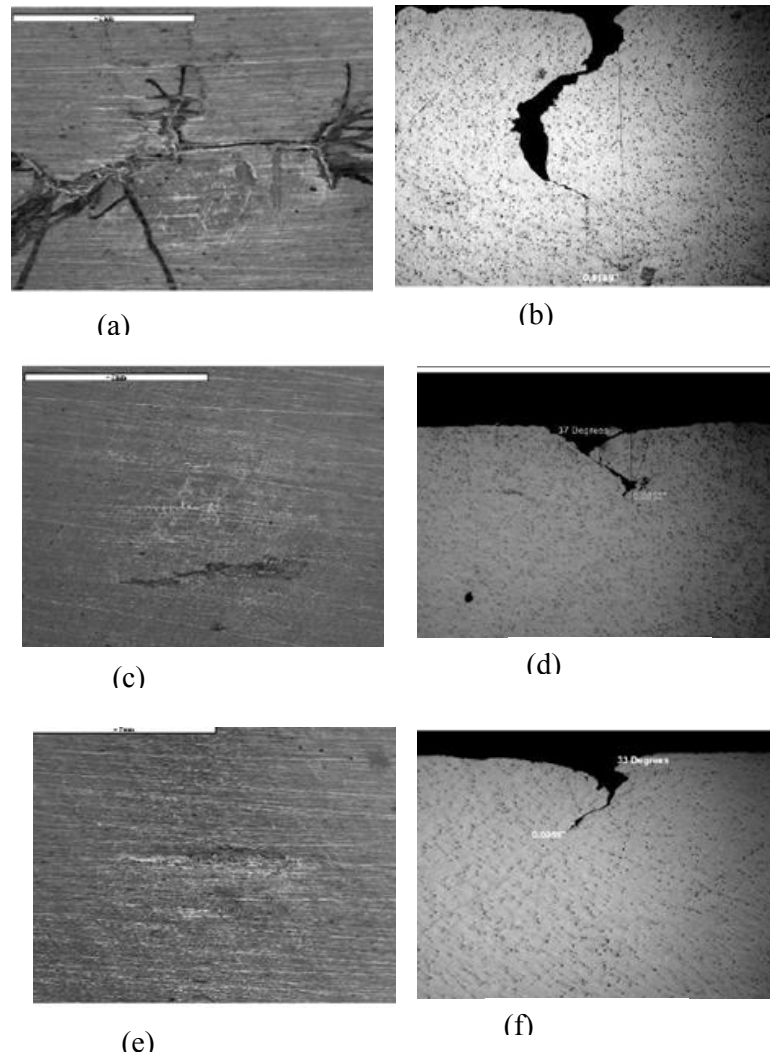


Figure 5. Optical microscopy analyses: (a) 600 °C, showing a crack on the sample's surface (b) 600 °C, Maximum crack depth is 1.626 mm, (c) 550 °C, revealing crack on the sample surface (d) 550 °C, Maximum crack depth is 0.135 mm, (e) 500 °C, showing crack on the sample surface (f) 500 °C, Maximum crack depth is 0.33 mm,

For each sample, the crack depths were measured in five planes (perpendicular to the surface) at successive distances of 0.2 mm. Column 4, Table 4, lists the maximum depth of the cracks for each sample. The experimental data in that table reveal that the cracks in the specimens exposed to 550 °C

and 500 °C are much shorter (maximum crack depth ~0.33 mm) than those for 600 °C (maximum crack depth ~1.6 mm).

Table 4 Crack-depth analysis for thermal-fatigue specimens

I.D	Test Temperature (°C)	Thermal Cycles	Maximum Crack Depth (mm)
Sample A	600	9503	1.626
Sample B	550	9865	0.025
Sample C	550	10,217	0.135
Sample D	500	10,010	0.330

Further experiments conducted on a second set of samples revealed, that at 450 °C one sample survived 20,000 thermal cycles with minimal cracking (maximum crack depth was ~0.01 mm), while another sample, exposed to half the number of thermal cycles (10,000 cycles) at that temperature, developed cracks ~0.33 mm deep. Microscopy analysis of this sample's surface further revealed several scale marks and surface defects (indicated by the yellow arrow in Fig.6(a)) surrounding one main crack. The surface of the other specimen with the ~0.01 mm deep crack showed no other damages (Fig. 6(c)).

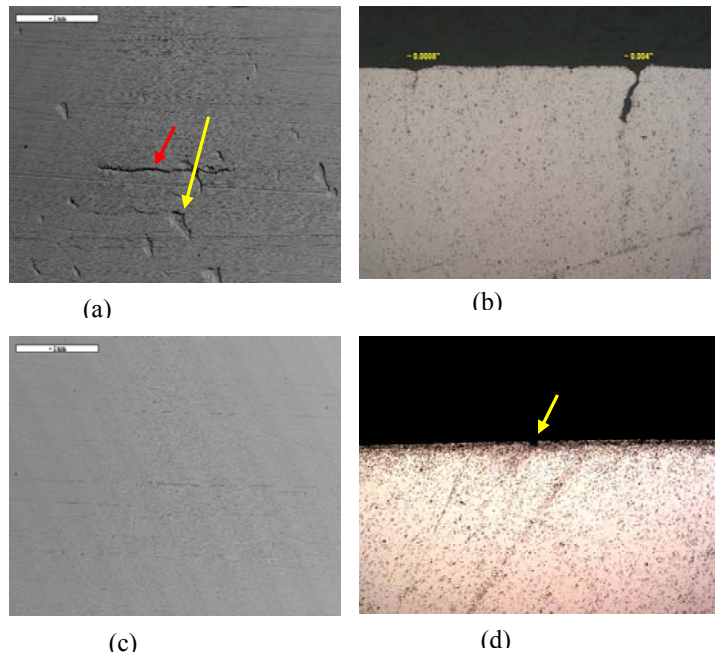


Figure 6. Optical microscopy analyses of samples exposed to a peak temperature of 450 °C: (a) Crack on one sample's surface: the main thermal-fatigue crack is shown by the red arrow, and the surrounding surface defect by the yellow arrow, (b) Maximum crack depth in this sample is 0.33 mm, (c) Crack on second sample's surface, and, (d) showing crack on the sample's surface, maximum crack depth ~0.01 mm

We believe that: (1) the initial surface defects could have acted as stress concentration points, and thus caused premature cracks in the samples. (2) As explained in Sec.2.2, in determining the x-ray source parameter (undulator gap value) that controlled the test temperature, we assumed that 20% of the beam power is lost due to scattering from the sample's surface. If the surface is rough, then there may be less scattering, leading to the deposition of a higher beam power. Under such circumstances, a specimen with uneven surface may develop surface cracks after far fewer thermal cycles. (3) If there are no pre-existing surface defects on the Glidcop sample's initial surface, then it seems to survive 10,000 cycles of an x-ray beam exposure at 450 °C. However the contradiction we found in our data suggests the need for more experiments at different surface roughnesses to assess the feasibility of operating at a beam condition that would result in a peak surface temperature of 450 °C.

3. Numerical Analysis

3.1. Fatigue life & crack size

For quantifying the thermal-fatigue life (in terms of number of thermal cycles) for the components used at the APS, it is important to identify a limit to crack size based on the component's ability to satisfy an important operating/design criteria. The cooling channels of these components lie at an average depth of 4-7 mm from the outer surface. To prevent water droplets from entering the high-vacuum storage ring, any cracks formed on the component's surface must not reach the walls of its cooling channel. The experimental data in Sec.2.2 demonstrate that except for the specimen exposed to a peak temperature of 600 °C, in all other specimens, the maximum depth of the cracks did not exceed 0.5 mm. Hence, from these experimental observations, we define a conservative limit of crack size of 0.5 mm, corresponding to 10,000 cycles of beam exposure. In future, we propose to study the mechanics of fracture to better understand the state of stress ahead of the crack's tip, thereby arriving at a more realistic size limit for cracks in the Glidcop components.

3.2. Non-linear FEA

To estimate the stress and strain fields developed in the thermal-fatigue specimens subsequently used to estimate, fatigue life, we numerically simulated the thermal-fatigue experiment using a nonlinear finite element (FEA) methodology. We undertook uncoupled thermal- and nonlinear stress analyses. These analyses are considered as uncoupled since the heat dissipation due to small-scale plastic yielding is negligible compared to the heating effect caused by exposure to the x-ray beam; also, the stresses and strains in the material result only from thermal loads. A typical uncoupled thermal stress analysis consists of (a) a transient thermal analysis, to compute the evolution of the temperature field in the model as a function of time and, (b) a stress- and-strain analysis to compute their corresponding fields, depending on the transient temperature's field.

3.2.1. Transient thermal analysis

In the transient thermal analysis, we applied the heat-flux boundary condition was applied in the form of a uniform heat flux over an area of $2.8 \text{ mm} \times 2.8 \text{ mm}$. We applied the uniform nodal- heat-flux values- 125-, 105- and 94- $\text{W}/\text{mm}^2\text{-}^\circ\text{C}$, resulting in a peak temperature of $600 \text{ }^\circ\text{C}$, $500 \text{ }^\circ\text{C}$, and $450 \text{ }^\circ\text{C}$ respectively. The heat transfer film coefficient on the surface of the cooling channel was assumed to be $0.015 \text{ W}/\text{mm}^2\text{-}^\circ\text{C}$ at a bulk reference temperature of $25.6 \text{ }^\circ\text{C}$. Table 5 gives the material properties of Glidcop Al-15 used for the thermal analysis[7].

Table 5 Thermo-mechanical properties for Glidcop Al-15 [7]

Parameters	Glidcop Al-15 (flat plate up to 10 mm thick)
Thermal conductivity, $\text{W}/(\text{m-K}) @ 293 \text{ K}$	365
Specific heat, $\text{J}/\text{kg-K}$	390
Density, Mg/m^3	8.90

Fig.7 depicts the evolution of temperature field as a function of time at the center of the x-ray beam's footprint. We then used, this transient temperature distribution in the thermal model as the input boundary condition for the subsequent nonlinear stress analysis.

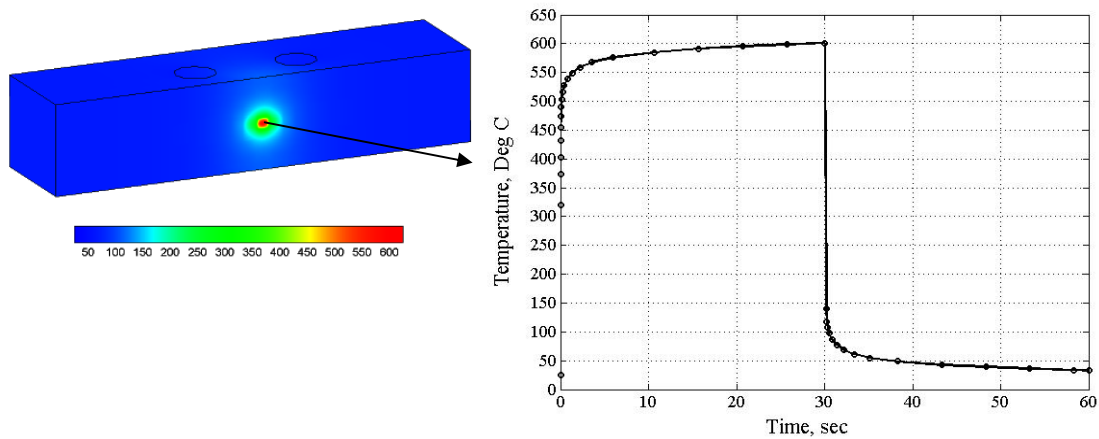


Figure 7. Evolution of temperature field as a function of time, for a peak power density of $125 \text{ W}/\text{mm}^2\text{-}^\circ\text{C}$ and peak temperature of $600 \text{ }^\circ\text{C}$

3.2.2. Elastic-plastic analysis

To model the cyclic elastic-plastic behavior of a material, one main requirement is to define the “hardening” rule, which describes how the yield stress evolves as a function of plastic straining and temperature. For metals such as dispersion-strengthened copper that are cyclically stable [8], the monotonic stress-strain behavior adequately describes their cyclic response [9]. To obtain this characteristic data for Glidcop Al-15, we carried out tensile tests on standard tensile Glidcop Al-15 specimens, 0.5 inches diameter, at the mechanical testing laboratory, Illinois Institute of Technology; bilinear kinematic hardening stress-strain curves for Glidcop Al-15 were obtained (Fig.8).

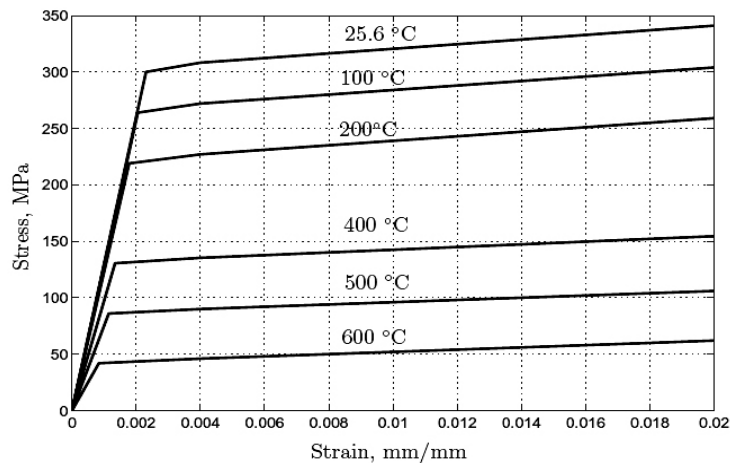
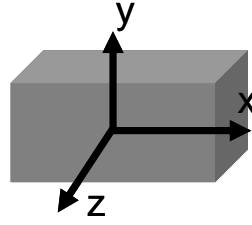
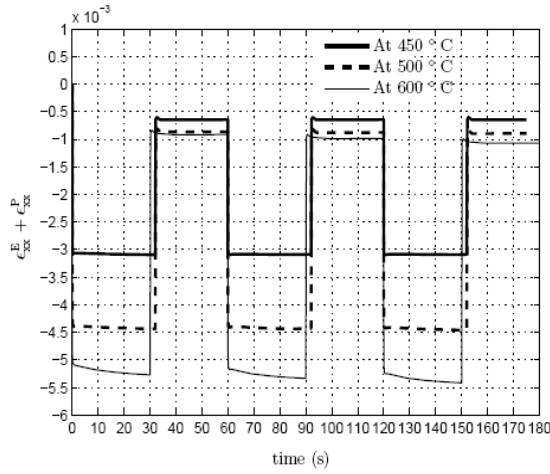


Figure 8. Bilinear kinematic hardening stress-strain curves for Glidcop Al-15

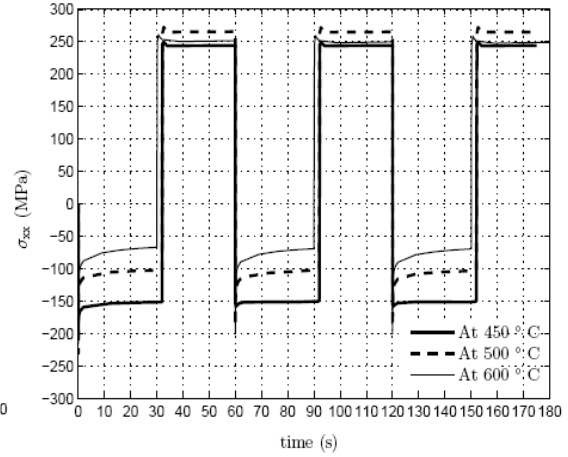
The load inputs to the stress analysis are the temperatures calculated in the thermal analysis at the various time steps. Because nonlinear stress analyses are time consuming, only three cycles of thermal loading were simulated, wherein each cycle consisted of a 30 seconds heating, and 30 seconds cooling. The mechanical stresses and strains that are function of the constraint on thermal expansion have their major components in the X-direction (Fig. 9(a)). The time variation in the mechanical strains and stress are shown in Fig. 9(b) and 9(c) respectively. The dark continuous curve, the dark broken curve, and the light continuous curve correspond to a peak temperature of 450 °C, 500 °C and 600 °C during the heating half of each cycle.



(a)



(b)



(c)

Figure 9. (a) Symbolic notation of the stress and strain components, (b) Time variation in the x-component of the total strain, and, (c) Time variation in the x-component of the stress.

3.2. Estimation of fatigue life

For multi-axial loading condition, it is important to consider the effect of the components of stress and strains and accordingly, we selected a fatigue life model called the Socie modified Smith-Watson-Topper model [10]. This model, based on observations of physical damage, postulates that a crack would grow perpendicular to the maximum tensile stress and the parameters that control damage are the maximum principal strain amplitude and the maximum principal stress on the maximum principal strain plane. The fatigue life is predicted by

$$\frac{\Delta \epsilon_t}{2} \sigma_{\max} = \frac{(\sigma_f)^2}{E} (2N_f)^{2b} + \sigma_f \epsilon_f (2N_f)^{b+c} \quad (2)$$

where $\Delta \epsilon_t$ is the principal total strain range, σ_{\max} is the maximum stress on the maximum principal strain plane, σ_f is the fatigue strength coefficient, E is the Young's modulus of the material, b is the fatigue strength exponent, ϵ_f is the fatigue ductility coefficient, c is the fatigue ductility exponent, and

N_f is fatigue crack initiation life. The parameters σ_f , b , ε_f and c defined as material properties, were obtained from the monotonic tensile stress strain data at room temperature using the empirical equations [9] given below.

$$\varepsilon_f = -\ln(1 - R.A.) \quad (3)$$

where R.A is the percentage reduction in area. For Glidcop Al-15 the value of R.A is $\sim 40\%$. For calculating the fracture strength σ_f , the average fracture stress σ_{avg} , was first computed using the empirical formula

$$\sigma_{avg} = -\sigma_u(1 + R.A.) \quad (4)$$

where σ_u is the ultimate tensile strength. For Glidcop Al-15, this value is 385 MPa. The fracture strength, σ_f then is obtained by correcting for necking using the Bridgeman's equation

$$\sigma_f = \frac{\sigma_{avg}}{\left(\left(1 + \frac{2R}{r_f} \right) \left(\ln \left(1 + \frac{r_f}{2R} \right) \right) \right)} \quad (5)$$

where

$$\frac{r_f}{2R} = 0.76 - 0.94(1 - \varepsilon_f) \quad (6)$$

The literature reports a value of -0.6 for the fatigue ductility exponent c of Glidcop Al-15 [8]. The published values of the fatigue strength exponent, b for metals vary from -0.08 to -0.15 [11]. Based on a published value -0.1 of b , for OFHC [12] and visual observations made in the experiment, the fatigue strength exponent (b) for Glidcop Al-15 was calibrated to -0.12. Table 6 summarizes the values of the fatigue material constants for Glidcop Al-15.

Table 6 Material Properties of Glidcop Al-15 for Fatigue Life Prediction

Parameter	Values
Reduction in area, %	40
Ultimate tensile strength, MPa	385
Fatigue ductility coefficient, ε_f	0.5
Fatigue strength coefficient, σ_f	503
Fatigue ductility exponent, c	-0.6
Fatigue strength exponent, b	-0.12

Finally, by substituting the fatigue material properties (Table.6) and the stress and strain results obtained from the FEA analysis in Eq.2, we assessed the fatigue life for different thermal-load conditions for peak power-densities of 125-, 105- and 94-W/mm² (Table.7).

Table 7 Undulator gaps and beam power corresponding to the estimated test temperatures

Peak Power Density (W/mm ²)	Total deposited Power (W)	Peak Temperature (°C)	σ_{xx} (MPa)	$\Delta\varepsilon_{xx}/2$ (%)	Life (Cycles)
125	980	600	250	0.221	5000
105	823	500	250	0.181	7000
94	736	450	250	0.125	19,000

4. Summary and Conclusions

All high-heat-load components used at the light sources are exposed to x-ray beam in a similar manner. In these components the thermal stresses and strains are generated mainly from the thermal constraint and at high heat loads will cause thermal fatigue cracks. To assess a safe beam operating condition for the synchrotron application, thermal-fatigue experiments were carried out on samples of Glidcop that underwent ~10,000 thermal cycles caused by exposure to an undulator x-ray of varying power densities viz., 94-, 105-, 115-, and 125-W/mm². The peak temperatures in the centre of the footprint at these power densities were 450, 500, 550, and 600 °C, respectively. Optical microscopy revealed that a sample subjected to a peak temperature of 600 °C corresponding to 125 W/mm² developed subsurface cracks of 1.6 mm. Since this exceeds the critical crack size of 0.5 mm that we defined in the Sec.3.1, a thermal loading condition in which a power density of 125 W/mm² at normal incidence results in a peak temperature of 600 °C is not a safe operating condition for the Glidcop Al-15 components. The experimental data shows that for power densities of 94-, 105-, and 115-W/mm² (450-, 500- and 550-°C respectively), the maximum crack depth in the specimen did not exceed 0.5 mm. These observations suggest that for temperatures below 550 °C, the initial surface cracks that form are arrested after reaching a certain size. To more realistically determine a critical limit on crack size, studies are needed of the effect of the temperature gradient from the surface to the cooling channel wall on the state of stress ahead of the crack's tip. This limit depends on the application criterion and the level of conservatism that the application can tolerate. For the light-source components, the most important criterion is that the cracks must not reach the cooling channel, typically at a depth of 4-7 mm. The experimental data coupled with the numerical result shows that for Glidcop Al-15 components, exposed to 10,000 cycles of an undulator x-ray with a peak power density of 94 W/mm² at normal incidence entailing a peak surface temperature of 450 °C, the maximum depth of the crack will be less than its critical size limit. In this work we have also used numerical methods for estimating fatigue life of the Glidcop samples. This model can be used for predicting fatigue life under any loading conditions.

5. Acknowledgements

The authors are grateful to the staff of the 26-ID beamline at APS, J. Maser, B. Stephenson and R. Winarski, for their support. Thanks are also due to J.Sullivan, R. Dortwegt, C. Putnam, M. Bracken, E. Theres, R. Bechtold and J.Collins for technical support in the beamline hutch, and to A. Woodhead for editing this paper. The work at Argonne was supported by the U.S. Department of Energy, Office of Science, Office of Basic Energy Sciences, under Contract W-31-109-ENG-38.

1.1. References

- [1] A.V.Nadkarni, ASM Metals Handbook-7, 9th Ed. (1984), 711-716
- [2] J.K. Tien, S.V. Nair, & V.C. Nardone, Flow and Fracture at Elevated Temperature, ASM (1985), 179-213.
- [3] W.J. Ostergren, J. Testing and Evaluation 76 (1954), 931-950.
- [4] D.C. Lord, & L.F. Coffin, Metallurgical Transactions 4 (1972), 1647-1654.
- [5] R.J.Dejus, I.B. Vasserman, & S. Sasaki, Argonne National Laboratory Technical Bulletin, ANL/APS/TB-45 (2002), http://www.aps.anl.gov/Facility/Technical_Publications/techbulletins.
- [6] L. Zhang, J.C. Biasci, S. Sharma, V. Ravindranath, & B. Rusthoven, Proc. MEDSI, Hyogo, Japan (2006)
- [7] J.D. Troxell, "Glidcop Dispersion Strengthened Copper: An Advanced Copper Alloy System for Aerospace and Defense Applications." Proc. IEEE Thirteenth Symposium on Fusion Engineering. 2 (1989), 761-765.
- [8] J. Robles, K.R. Anderson, J.R. Groza, J.C. Gibeling, "Low-Cycle Fatigue of Dispersion-Strengthened Copper," Metall. Mater. Trans., 25A (1994), 2235.
- [9] M.R. Mitchell, "Fundamentals of Modern Fatigue Analysis for Design," ASM Handbook–Fatigue and Fracture, v. 19, pp. 227-249.
- [10] A. Fatemi, D.F. Socie, "A Critical Plane Approach to Multiaxial Fatigue damage including out-of-phase loading," Fatigue Fract. Eng. M. 11 (1988) 149
- [11] R. Hertzberg, Deformation and Fracture Mechanics of Engineering Materials, New York: Wiley (1989), Ch 12.